sciendo

Int. J. Appl. Math. Comput. Sci., 2022, Vol. 32, No. 3, 441–454
DOI: 10.34768/amcs-2022-0032

amcs

A SINGLE IMAGE DEBLURRING APPROACH BASED ON A FRACTIONAL ORDER DARK CHANNEL PRIOR

XIAOYUAN YU [a], WEI XIE [a,b,*], JINWEI YU [a]

[a] School of Automation Science and Engineering
South China University of Technology
Wushan Road, Tianhe District, 510641 Guangzhou, China
e-mail: yuwspg@163.com

[b] Key Laboratory of Autonomous Systems and Networked Control
Ministry of Education
Wushan Road, Tianhe District, 510641 Guangzhou, China

The dark channel prior has been successfully applied to solve the blind deblurring problem on different scene images. Since the dark channel of the blurry-noise image is similar to that of the corresponding clear image, the sparsity of the dark channel is less effective for image blind deblurring. Inspired by the fact that a fractional order calculation can inhibit the noise and preserve the texture information of the image, a fractional order dark channel prior is proposed for image deblurring in this paper. It is appropriate for kernel estimation where input images and intermediate images are processed by using a fractional order dark channel prior. Furthermore, the non-convex problem is solved by the half-quadratic splitting method, and some metrics are used for deblurring image quality assessment. Finally, quantitative and qualitative experimental results show that the proposed method achieves state-of-the-art results on synthetic and real blurry images.

Keywords: blind image deblurring, fractional order dark channel prior, non-convex problem.

1. Introduction

The single image blind deconvolution (SIBD) algorithm is very significant in computer vision, being applied to camera image stabilization, medical image clarity, security monitoring, etc. Particularly, the blurring issue of images captured by hand-held cameras has become more common, which is caused by the relative motion between the object and the camera during camera exposure (Gao *et al*., 2019). On the other hand, it is always difficult and unrepeatable to make a secondary image of the same scene. Therefore, it is necessary that blurry images can be restored to relatively high-resolution and discernible high-quality images.

If the blur is uniform and spatially invariant, then the blurry image model can be described as follows:

$$b = k \otimes f + n, \tag{1}$$

where b, k, f, and n denote the blurry image, blur kernel, latent image and noise, respectively. Moreover, $\otimes$ denotes the convolution operator. The purpose of single image deblurring is to estimate the relative blur kernel k and the latent image f from the single blurry image b simultaneously. It is a highly ill-posed problem because there are many diverse versions of latent image f and blur kernel k, which can lead to the same blur image b.

The challenge of SIBD in the past decade has been mainly focused on model establishment and problem optimization. There are some significant algorithms in SIBD (or motion deblurring), including efficient inference methods (Shan *et al*., 2008; Cho and Lee, 2009; Xu and Jia, 2010; Levin *et al*., 2011; Xie, 2016; Kotera *et al*., 2017), various image priors (Wang *et al*., 2018; Yan *et al*., 2017; Joshi *et al*., 2009; Ren *et al*., 2016; Kotera *et al*., 2013; Yin *et al*., 2014), L_0 norm form (Xu *et al*., 2013; Pan *et al*., 2014a; Li and Lu, 2016), and the camera anti-shake algorithm (Fergus *et al*., 2006). Among them, image deblurring methods based on image sparsity are an important aspect. For example, some image deblurring methods (Pan *et al*., 2018; Xu *et al*., 2013) are proposed

*Corresponding author

exploiting image sparsity. Pan *et al*. (2018) set forth an image deblurring algorithm based on the dark channel prior (DCP). However, since significant noise changes the sparsity of the dark-channel result of a blurry image, the estimate of the blur kernel and the intermediate image would be affected seriously. Therefore, fusing image-processing approaches into the DCP may yield accurate estimates from blurry images.

In this paper, we propose an image blind deblurring method based on a fractional order dark channel prior (FODCP) which uses a fractional order operator to process blurry images. We observe that the dark channel result of the blurry image becomes darker when the blurry image has significant noise or less bright pixels. Further, the dark-channel result of the noise-blurry image is similar to that of the clear image. Thus, the dark-channel prior is less effective for restoring the noise-blurry image directly. By contrast, we find that fractional order theory, including the fractional differential operator and fractional integral operator, can effectively process the anomaly signal (Li and Xie, 2015; 2016). Therefore, the proposed FODCP can produce the robust dark channel of a noise-blurry image and estimate the blur kernel by restraining the noise of the image. Further, the L_0 regularized term is used for computing the sparsity of the FODCP according to Pan *et al*. (2018); the optimization with the L_0 regularization term is implemented by using the half-quadratic splitting method. The contributions of this paper are as follows:

- We analyze the low effect of the dark channel prior when the blurry image includes typical noise (such as Gaussian noise).
- For the blurry image, we propose a fractional order dark channel prior (FODCP), which can suppress the noise of image and obtain a more significant dark channel robustly.
- We develop an efficient framework for solving the optimization problem of the proposed blind deblurring method.

The paper is organized as follows. The related works on image deblurring and fractional order calculation are reviewed in Section 2. Section 3 introduces and analyzes the proposed FODCP. Section 4 shows how to solve the single image deblurring problem based on FODCP. In Section 5, experimental results regarding the proposed method and other state-of-the-art approaches are demonstrated. Finally, Section 6 presents the conclusions.

2. Related work

We discuss the related work on image deblurring methods and introduce the fractional order method for the image vision problem.

2.1. Image deblurring methods. Recently, deep--learning methods have been proposed for solving the image deblurring problem (Gong *et al*., 2017; An *et al*., 2020). For instance, Li *et al*. (2019) combined the traditional deblurring framework to estimate the latent image after learning the image prior by a non-linear DNN network. Furthermore, end-to-end models are used for directly obtaining deblurring results. Kupyn *et al*. (2018) proposed an image deblurring network based on conditional generative adversarial networks, which can reach a higher processing speed. Further, edge information (Zhichao *et al*., 2019) or semantic information (Fuhai *et al*., 2019) of the input image are extracted to modulate the intermediate feature of a deblurring network. Zhang *et al*. (2019) proposed a deep hierarchical multi-patch network for image deblurring, which can represent the fine-to-coarse hierarchical feature. However, these methods are designed based on the black-box principle, which means that it is hard to explain the mechanism behind their operation.

Therefore, in order to estimate the latent image and the blur kernel from the blurry image, there are various deblurring methods adding some image priors, which can avoid the trivial solutions for the blur kernel.

Some papers proposed a deblurring method based on different image priors. Chen *et al*. (2010) proposed a method combining an image gradient histogram to fit the distribution of the image gradient and used that for image deblurring. Shan *et al*. (2008) designed a two piece-wise continuous function to fit the logarithmic gradient distribution of natural images and used it to deblur an image. Fergus *et al*. (2006) used a zero-mean mixture of Gaussians to represent the distribution of gradient magnitudes of the image, and image deblurring was proposed by the maximum *a-posteriori* (MAP) solution. In the work of Kotera *et al*. (2013), heavy-tailed priors of the image and alternating MAP solutions were used to construct the deblurring image framework whose non-convex optimizing problem was solved by the augmented Lagrangian method.

Since the above natural image priors favor clear images, rather than blurry ones, heuristic edge selection has been used for estimating the kernel. Cho and Lee (2009) proposed a multi-scale framework by predicting solid edges of the intermediate image, which can accelerate the estimation of the blur kernel. Xu and Jia (2010) set forth a two-phase method for kernel estimation by further expansion of the results of Cho and Lee (2009). Sun *et al*. (2013) proposed a patch prior by constructing a set of edge patches from example patches and used that to recover the intermediate image. Further, Lai *et al*. (2015) introduced intermediate shape patches for image deblurring by added normalized color-line priors into Sun's method (Sun *et al*., 2013). However, these methods would be inefficient when there are not enough

step edges in the input image.

On the other hand, low-rank priors of the image have been developed and successfully applied to image modeling. Pan *et al*. (2014b) estimated the blur kernel based on salient edges and a low rank prior. Yan *et al*. (2017) observed low-rank properties of image intensity and image gradient maps and used these to recover the blur kernel and an intermediate image. In addition, Wang *et al*. (2018) proposed an elastic-net regularization of singular values computed from similar patches of an image and used it to guide the kernel estimation. However, a low rank prior would be a problem when an image contains rich textures located in most regions or nearly in the whole image.

Recently, L_0 sparsity has been developed as the regularization term and used for image deblurring (Xu *et al*., 2013). Pan *et al*. (2014a) proposed a method for text image deblurring, which used the L_0 regularization term for image intensity and image gradient. Furthermore, Li and Lu (2016) introduced a blind image motion deblurring method by adopting L_0 regularized priors both in the kernel and latent image estimation. Pan *et al*. (2018) proposed a deblurring method by using the dark channel prior and an L_0 regularization term for the image gradient and the dark channel image. Pan *et al*. (2018) proved that the dark channel of the clear image was sparse, and it was different from that of a blurry image. However, the dark channel prior is less effective for estimating the blur kernel and the intermediate image when the input image includes significant noise. Therefore, this paper promotes the method of Pan *et al*. (2018), which can improve the quality of the deblurring image.

2.2. Fractional order calculus. Fractional order calculus is a generalization of the integer order calculus (Matychyn and Onyshchenko, 2021). It is a mathematical problem for studying the properties and applications of an arbitrary fractional order operator. In recent years, fractional order calculus has been successfully applied to image processing. Jia and Pu (2008) argued that the performance image edge detection using fractional differentials is better than that of integer order mask operators. Recently, Li and Xie (2015; 2016) proposed an approach for defining the fractional order value adaptively and used it for the denoising and enhancement of medical images. It is shown that the changes in the signal using fractional order processing are nonlinear. For example, when fractional order calculus is used to enhance the signal, the high-frequency component would be nonlinearly enhanced, and the low-frequency component of the signal would be preserved as soon as possible. Fractional order calculus is used for restraining noise and preserving textures. In order to enforce sparsity and the constraint of the dark channel of the image, we propose an FODCP. In this paper, fractional order calculus is used to restrain the noise and preserve textures, which effectively extract the dark channels of input and intermediate images.

3. Fractional order dark channel prior

In this section, we first describe the theory. Then, we characterize the dark channel prior based on the work of Pan *et al*. (2018). Finally, we introduce the theory of the proposed FODCP.

3.1. Fractional order theory. Fractional order calculation, whose order is arbitrary, is an extension of integer calculation. There are mainly three defining formulas of fractional order calculation, including the Grunwald–Letnikov (G–L) definition, the Riemann–Liouville (R–L) definition, and the Caputo definition. Since G–L is the most popular definition used in digital image processing, we employ fractional order calculation with the G–L definition in the paper. Taking a one-dimensional signal $f(t)$ as an example, the G–L definition of signal $f(t)$ can be written as follows:

$$D^{v}_{\text{G-L}} f(t) = \lim_{h\to 0} h^{-v} \sum_{j=0}^{q} (-1)^j \binom{v}{j} f(t-jh), \qquad (2)$$

where $q = [(b-a)/h]$, $[x]$ denotes the operator for extracting the integral part of input x, and h denotes the step. Here

$$\binom{v}{j} = \frac{\Gamma(v+1)}{j!\Gamma(v-j+1)}.$$

$\Gamma(x)$ denotes the Gamma function

$$\Gamma(x) = \int_0^{\infty} e^{-t} t^{x-1}\,\mathrm{d}t.$$

In order to use fractional order theory for image processing, (2) should be rewritten as an algebraic expression. For the one-dimensional signal $f(t)$, we get the following form of (3):

$$\begin{aligned} D^{v}_{\text{G-L}} f(t) = {} & f(t) + (-v) f(t-1) \\ & + \frac{(-v)(-v+1)}{2} f(t-2) \\ & + \cdots + \frac{\Gamma(-v+1)}{n!\Gamma(-v-n+1)} f(t-n). \end{aligned} \qquad (3)$$

When the order is set as $v > 0$, $D^{v}_{\text{G-L}}$ denotes the fractional differential operator of order v. Otherwise, $D^{v}_{\text{G-L}}$ denotes the fractional integral operator of order v when the order is set as $v < 0$.

Then, we compute the fractional order of eight directions at each pixel. Finally we construct the fractional order operator by fusing the fractional order calculation of eight directions, cf. Li and Xie (2015;

2016). The fractional operator $D^{v}_{\text{G-L}}$ can be constructed as follows:

$$D^{v}_{\text{G-L}} = \xi^{v} \times \begin{bmatrix} V & 0 & V & 0 & V \\ 0 & -v & -v & -v & 0 \\ V & -v & 8 & -v & V \\ 0 & -v & -v & -v & 0 \\ V & 0 & V & 0 & V \end{bmatrix}, \tag{4}$$

where $V = \left(v^2 - v\right)/2$,

$$\xi^{v} = \frac{1}{8 - 12v + 4v^2}.$$

If an input $s(t)$ is a square-integrable energy signal, the frequency response of $s(t)$ with a fractional differential operator and a fractional integral operator is described as shown in Figs. 1(a) and (b), respectively. According to Fig. 1(a), the fractional differential operator can retain the low-frequency part (textures) of signals (image) while the fractional differential operator enhances the high-frequency part (edges) of the signal. In addition, the low-frequency part of the image can be enhanced as far as possible when the fractional integral operator inhibits the noise of the image, as shown in Fig. 1(b).

3.2. Fractional order dark channel prior. The dark channel (He *et al*., 2009) of image f is defined as follows:

$$D\left(f\right)\left(x\right) = \min_{y \in \Omega(x)} \left(\min_{c \in \{r,g,b\}} f^{c}\left(y\right) \right), \tag{5}$$

where x and y are the pixel location, f^{c} denotes the c-th channel of the image f, and $\Omega(x)$ is a local patch of the image at x. If the image is a gray one, its dark channel only processes one channel. According to He *et al*. (2009), the dark channel of a natural image, like a free fog image and clear image, is close to zero. Further, Pan *et al*. (2018) observed that the dark channel of a blur image has fewer dark pixels than the one of a clear image and proposed a blind deblurring method based on the dark channel prior.

However, we observe that most pixels in the dark channel of a noisy blurry image would become darker when the blurry image has some significant noise. To explain this phenomenon, we define the blur operator and analyze the properties of noise-free blurry images and a noise-blurry image.

For blurry images B, each pixel of B is defined a linear combination of a patch of clear image I and a blur kernel k, which can be written as

$$B\left(x\right) = \sum_{z \in N_k} I\left(x + \left[\frac{s}{2}\right] - z\right) k\left(z\right)$$

subject to

$$k\left(z\right) \geq 0, \quad \sum_{z \in N_k} k\left(z\right) = 1, \tag{6}$$

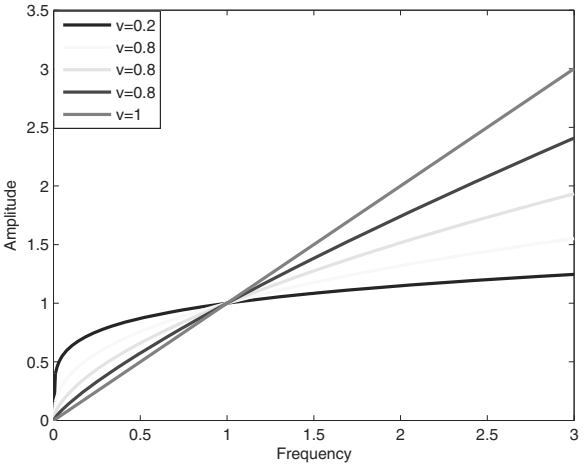

(a)

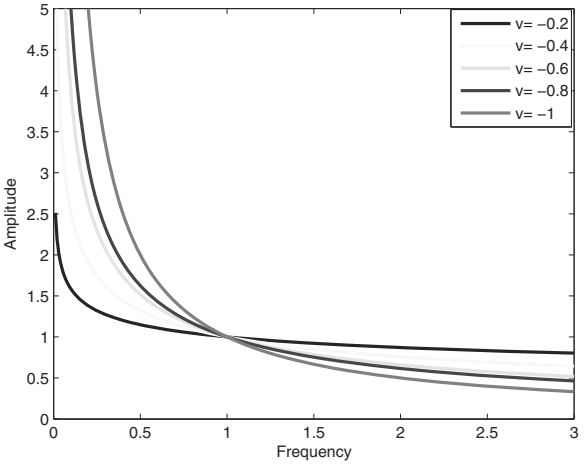

(b)

Fig. 1. Frequency response of signal $s(t)$ with each fractional order based on a different operator: fractional differential operator (a), fractional integral operator (b).

where N_k and s denote the domain and size of blur kernel k, and $[\cdot]$ denotes the rounding operator.

To generate the noise-blurry image, we use the `imnoise` function of the MATLAB software for simulating random Gaussian noise. According to the MATLAB file, the Gaussian noise n in this paper is defined as follows:

$$n\left(x\right) = M + \sqrt{\sigma} \times \texttt{randn}(a), \tag{7}$$

where M and σ denote the mean and the variance of n, respectively, and $\texttt{randn}(a)$ denotes the function that produces a matrix of size $a \times a$ with standard normal distribution.[1] Then, the noise-blurry image $B_n(x)$ is defined that the blurry image $B(x)$ with added Gaussian noise $n(x)$ (assumed that the mean of n is 0 and the

[1] In fact, the elements of $\texttt{randn}(a)$ have a high probability of being negative.

variance of n is σ in this paper). It can be expressed as follows:

$$B_n(x) = B(x) + n(x) \tag{8}$$

Next, we analyze why the noise-blurry image $B_n(x)$ would have more dark pixels after processing by the DCP.

Proposition 1. *$N(x)$ denotes a patch centered at pixel x whose size is the same as that of the blur kernel. Let $D(f)(x)$ denote the dark-channel operator of signal f. We have*

$$D\left(I\right)\left(x\right) \leq D\left(B_n\right)\left(x\right) \leq D\left(B\right)\left(x\right). \tag{9}$$

Proof. The detailed derivation can be found in the work of (Pan *et al.*, 2018). Firstly, based on the definition of (6), we have

$$\begin{aligned} B(x) &= \sum_{z\in\Omega_k} I\left(x + \left[\frac{s}{2}\right] - z\right)k\left(z\right) \\ &\geq \sum_{z\in\Omega_k} \min_{y\in N(x)} I(y)k\left(z\right) = \min_{y\in N(x)} I(y). \end{aligned} \tag{10}$$

Thus, it is clear that

$$D\left(I\right)\left(x\right) \leq D\left(B\right)\left(x\right). \tag{11}$$

Similarly, we can obtain that

$$D\left(I\right)\left(x\right) \leq D\left(B_n\right)\left(x\right). \tag{12}$$

Secondly, we define two positive numbers, ε_1 and ε_2. Based on (7), we have $-\varepsilon_1\sqrt{\sigma} \leq n(x) \leq \varepsilon_2\sqrt{\sigma}$. Thus, we have $B(x) - \varepsilon_1\sqrt{\sigma} \leq B_n(x) \leq B(x) + \varepsilon_2\sqrt{\sigma}$. In this paper, the size of $N(x)$ is set as 35×35. It is reasonable to assume that there are some pixel values of $B_n(x)$ that are not larger than the value of blurry image B on the domain $N(x)$. Based on statistical regularity and the definition of the dark channel, we have

$$\begin{aligned} D\left(B_n\right)\left(x\right) &= D\left(B+n\right)\left(x\right) \\ &= \min_{y\in N(x)}\left[\min_{c\in\{r,g,b\}}\left(B^c\left(y\right) + n^c\left(x\right)\right)\right] \\ &\leq \min_{y\in N(x)}\left[\min_{c\in\{r,g,b\}} B^c\left(y\right)\right] = D\left(B\right)\left(x\right). \end{aligned} \tag{13}$$

Based on (11)–(13), we can obtain $D\left(I\right)\left(x\right) \leq D\left(B_n\right)\left(x\right) \leq D\left(B\right)\left(x\right)$. ∎

Note that when the blurry image is corrupted with significant noise, the pixel values of the dark channel of the blurry-noise image tend to become smaller, as shown in Fig. 2. Therefore, after combining some properties of fractional order calculation, we propose an FODCP to obtain the robust dark-channel result, improving the quality of the estimated kernel and image. The definition of the FODCP is as follows:

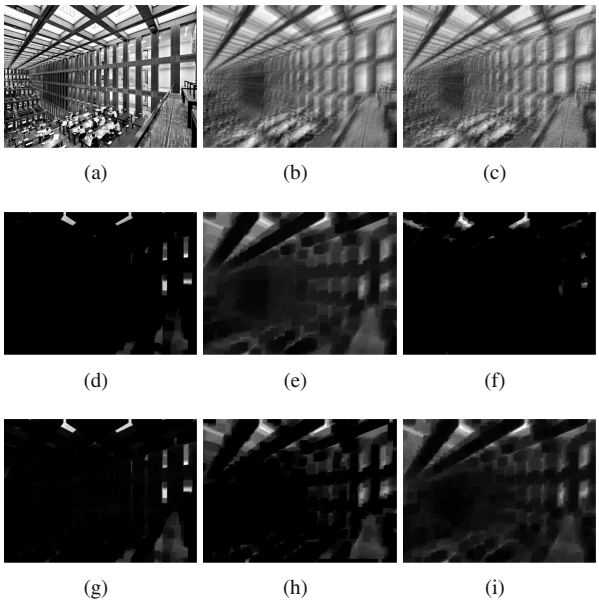

Fig. 2. Dark-channel results using DCP and FODCP: clear image (a), blurry image (b), blurry image with Gaussian noise (c); (d)–(f) are dark-channel results using DCP with (a)–(c), respectively; (g)–(i) are dark-channel results using FODCP with (a)–(c), respectively.

$$D\left(f_v\right)\left(x\right) = \min_{y\in\Omega(x)}\left(\min_{c\in\{r,g,b\}} f_v^c\left(y\right)\right), \tag{14}$$

where $f_v{=}D^v_{\text{G-L}} \otimes f$.

To explain why the FODCP can effectively process the blurry image with or without significant noise, we introduce an example by using the DCP and an FODCP (the value v is set as -0.6) for the noise-free and the noise blurry image, respectively. We choose one picture from the data set (Lai *et al.*, 2016). On the one hand, if the blurry image has less significant noise, we find that the result produced by the FODCP is similar to the one by the DCP, as shown in Fig. 2(b). On the other hand, if the blurry image is influenced by considerable Gaussian noise, the dark channel of the noise-blurry image produced by the DCP has fewer bright pixels and it is similar to a clear image. Thus, this dark channel is unable to help the estimation of the kernel and the intermediate image. In comparison, the dark channel of the noisy-blurry image produced by the FODCP is similar to the bottom one of Fig. 2(b). Therefore, the FODCP is robust in obtaining the dark-channel result irrespective of whether the noise-blurry image or the noise-free blurry image is processed.

4. Proposed method

In this section, we propose an image deblurring method using the FODCP. Then, we set forth optimization for estimating the blur kernel.

4.1. Proposed deblurring model. According to the MAP framework and the image blur model of (1), we construct the deblurring problem as follows:

$$\begin{aligned}\{f,k\} &= \arg\max_{f,k} p(f,k|b)\\ &= \arg\max_{f,k} p\left(b|f,k\right)p\left(f\right)p\left(k\right).\end{aligned} \tag{15}$$

We take the negative log-likelihood of (15) and get the following deblurring model:

$$\{f,k\} = \arg\min_{f,k} l(f\otimes k,b) + \gamma\phi(k) + \lambda\varphi(f). \tag{16}$$

The first term of (16) is named the data fidelity term, which means that the recovered image is consistent with the input image. According to Shan *et al*. (2008), we use the L_2 norm to penalize the difference between $f\otimes k$ and b in this paper,

$$l\left(f\otimes k,b\right) = \left\|f\otimes k-b\right\|_2^2. \tag{17}$$

The second term of (16) denotes the kernel prior, which is used to enforce the blur kernel. Similarly to Cho and Lee (2009), the L_2 norm is used to estimate the blur kernel as follows:

$$\phi\left(k\right) = \left\|k\right\|_2^2, \quad k_i \geq 0, \quad \sum_i k_i = 1. \tag{18}$$

As shown by Cho and Lee (2009), who studied the kernel prior and the data fidelity term, the kernel can be constructed easily by the fast Fourier transform (FFT).

The last term of (16) is the image prior. Due to the effect of the noise-blurry image, the dark-channel result is close to that of a clear image, which is unable to help the estimation of the kernel and the intermediate image. The proposed FODCP can solve this problem. After processing the image with the FODCP, the effect of the dark channel is robust. In addition, we consider the sparsity of the image gradient (Pan *et al*., 2014b) and use it for image deblurring. Therefore, the image prior term can be represented as follows:

$$\varphi\left(f\right) = \sigma\|\nabla f\|_0 + \lambda\|D(f_v)\|_0, \tag{19}$$

where $\nabla = [\nabla_h, \nabla_v]^T$ denote the gradient operators and the form of $D\left(f_v\right)$ is the same as that of (14). It is useful to estimate the blur kernel and intermediate image by using the L_0 norm for denoting the sparsity of the image gradient and the fractional order dark channel.

4.2. Optimization. Based on the previous discussion, we can derive the following minimization formula (20) for image deblurring:

$$\begin{aligned}\{f,k\} = \arg\min_{f,k} &\left\|f\otimes k-b\right\|_2^2\\ &+\lambda\|\nabla f\|_0 + \mu\|D(f_v)\|_0 + \gamma\left\|k\right\|_2^2,\end{aligned} \tag{20}$$

Alternating optimization of f and k in an iterative process is a successful approach for image deblurring. From (20), we can respectively solve the estimation of the latent image and the blur kernel as follows:

$$\begin{aligned}\bar{f} = \arg\min_{f} &\left\|f\otimes k-b\right\|_2^2 + \lambda\|\nabla f\|_0\\ &+\mu\|D(f_v)\|_0,\end{aligned} \tag{21}$$

$$\bar{k} = \arg\min_{k} \left\|f\otimes k-b\right\|_2^2 + \gamma\left\|k\right\|_2^2. \tag{22}$$

4.2.1. Estimation of the latent image. In this subproblem, the blur kernel is fixed. In order to optimize the latent image, we use the half-quadratic splitting method (Xu *et al*., 2013) by adding two auxiliary variables g and l into (21). The function (21) can be rewritten as follows:

$$\begin{aligned}\{\bar{f},\bar{g},\bar{l}\} = \arg\min_{f,g,l} &\left\|f\otimes k-b\right\|_2^2 + \alpha\left\|\nabla f-g\right\|_2^2\\ &+\beta\left\|D(f_v)-l\right\|_2^2 + \lambda\|g\|_0 + \mu\|l\|_0,\end{aligned} \tag{23}$$

where α, β, λ, and μ are positive parameters. As $\alpha,\beta\to\infty$, the estimate f of function (23) is close to the estimate f of the function (21).

Firstly, we fix g and l to determine the latent image f. We get

$$\begin{aligned}\bar{f} = \arg\min_{f} &\left\|f\otimes k-b\right\|_2^2\\ &+\alpha\left\|\nabla f-g\right\|_2^2 + \beta\left\|D(f_v)-l\right\|_2^2,\end{aligned} \tag{24}$$

where $f_v = D_{\text{G-L}}^v \otimes f$.

For the optimization of (24), we modify $D(f_v)$. According to Pan *et al*. (2018), the dark channel prior function $D(f)$ is nonlinear and should be replaced with an equivalent linear operator M. The operator M is a mapping matrix used to map the pixel to its dark channel. M is defined as follows:

$$M(x,y) = \begin{cases} 1, & y = \arg\min\limits_{y\in\Omega(x)} f(y),\\ 0, & \text{otherwise.}\end{cases} \tag{25}$$

In this paper, a dark channel prior is added the fractional operator to improve the blurring image's dark channel. Therefore, we should compute the mapping matrix M_D^v of $D(f_v)$ after the fractional operator

processes the intermediate image. The function (24) can be rewritten as follows:

$$\begin{aligned}\bar{f} = \arg\min_{f} &\|f \otimes k - b\|_2^2 \\ &+ \alpha \|\nabla f - g\|_2^2 + \beta \|M_{D^v} f - l\|_2^2 ,\end{aligned} \tag{26}$$

where $M_{D^v} f{=}M(D^v_{\text{G-L}} \otimes f)$. According to Shan *et al.* (2008), the latent image f of the function (26) can be computed by the FFT,

$$\overline{f} = F^{-1}\left(\frac{\overline{F(k)} \odot F(b) + \alpha F_g + \beta F_{Ml}}{\overline{F(k)} \odot F(k) + \alpha F_\nabla + \beta F_M}\right), \tag{27}$$

where $F_g{=}\overline{F(\nabla_h)} \odot F(g_h) + \overline{F(\nabla_v)} \odot F(g_v)$, $F_{Ml} = \overline{F(M_{D^v})} \odot F(l)$, $F_M = \overline{F(M_{D^v})} \odot F(M_{D^v})$, $F_\nabla{=}\overline{F(\nabla)} \odot F(\nabla)$, $\nabla{=}[\nabla_h, \nabla_v]^T$ denote the gradient operators. $F(\cdot)$ and $F^{-1}(\cdot)$ are the FFT and the inverse FFT, respectively. Here $\odot$ denotes the element-wise multiplication operator and $\overline{(\cdot)}$ the conjugate operator.

Secondly, the auxiliary variables g and l can be computed separately given f. The functions for estimating g and l are as follows:

$$\bar{g} = \arg\min_{g} \alpha \|\nabla f - g\|_2^2 + \lambda \|g\|_0, \tag{28}$$

$$\bar{l} = \arg\min_{l} \beta \|D(f_v) - l\|_2^2 + \mu \|l\|_0. \tag{29}$$

Because (28) and (29) are pixel-wise minimization problems, the estimates of g and l can be obtained using the technique proposed by Pan *et al.* (2014b)

$$\bar{g} = \begin{cases} \nabla f, & |\nabla f|^2 \geq \frac{\lambda}{\alpha}, \\ 0, & \text{otherwise}, \end{cases} \tag{30}$$

and

$$\bar{l} = \begin{cases} D(f_v), & |D(f_v)|^2 \geq \frac{\mu}{\beta}, \\ 0, & \text{otherwise}. \end{cases} \tag{31}$$

4.2.2. Estimation of the blur kernel. In this subproblem, the blur kernel is computed given f. According to Cho and Lee (2009), the blur kernel can be better estimated based on the gradient image. Therefore, we use the gradient operator and the L_2 norm to estimate the blur kernel as follows:

$$\bar{k} = \arg\min_{k} \|\nabla f \otimes k - \nabla b\|_2^2 + \gamma \|k\|_2^2 . \tag{32}$$

According to existing methods, the function (32) can be computed by the FFT,

$$\bar{k} = F^{-1}\left(\frac{\overline{F(\nabla f)} \odot F(\nabla b)}{\overline{F(\nabla f)} \odot F(\nabla f) + \gamma}\right). \tag{33}$$

Algorithm 1. Deblurring by the proposed algorithm.

Require: The blurry image b; Size of kernel k, $M \times M$; the initial blur kernel k_0 is set as function δ; the maximum fractional order $v_{\max}$; the minimum fractional order $v_{\min}$

Ensure: The estimate of kernel k; the estimate of latent image f.

create the image pyramid $\{b_0, b_1, \ldots, b_n\}$;
compute the step of changing fractional orders $T = (v_{\max} - v_{\min})/n$ (n is decided by M according to Fergus *et al.* (2006));
for $i = 1, 2, \ldots, n$ (coarse level to fine level) **do**
  $v = v_{\min}$;
  for $j = 1, 2, \ldots, 5$ **do**
    while $\beta < \beta_{\max}$ **do**
      estimate l by optimizing (31);
      $\beta \Leftarrow 2\mu$;
      while $\alpha < \alpha_{\max}$ **do**
        $\alpha \Leftarrow 2\lambda$;
        estimate g by optimizing (30);
        estimate f by optimizing (27);
        $\alpha \Leftarrow 2\alpha$;
      end while
      $\beta \Leftarrow 2\beta$;
    end while
    estimate k by optimizing (33);
    $\mu \Leftarrow \max\{\mu/1.1, \mu_0\}$;
    $\lambda \Leftarrow \max\{\lambda/1.1, \lambda_0\}$;
  end for
  $v \Leftarrow v_{\min} + Ti$;
end for

Similarly to state-of-the-art methods, a multi-scale blind deconvolution framework is used for optimizing the proposed method. The value of the computed kernel is set as non-negative (the negative value is set as 0), and normalization (the sum of all kernels k should equal 1) in every scale. This means that the blur kernel and the intermediate image are estimated from coarse-scale to fine-scale. Thus, the value of fractional order v undergoes an adaptive change based on the image (kernel) scale in this framework. When the input image is the most coarse-scale, the fractional order v is set as -0.6, which can inhibit the noise of the input image at the beginning. Further, the fractional order v would be increased linearly when the scale of intermediate image is bigger. It is to be noted that the value of v is set as 0.8 when the image is at fine-scale. In this way, the noise of the input image can be inhibited at the beginning, and the details of the image can be enhanced, which is effective for estimating the blur kernel. The main steps of the proposed method are shown in Algorithm 1.

4.2.3. Final image restoration. Once the kernel k is estimated, there are numerous non-blind deblurring methods to restore the final image. On the other hand, the function (27) also can be used to estimate the latent image. However, if the blurry input image contained considerable noise, the restored latent image would consist of some outliers based on the above methods. To obtain a latent image with clear details, we introduce the non-blind deblurring method (Zhong *et al*., 2013) for the restored latent image after obtaining the final kernel.

5. Experimental results

In this section, we analyze some experiments on synthetic and real images to show the efficiency of the proposed algorithm. It should be noted that the metric results from objective assessment methods would not change with the subjective factors. Thus, we compare other deblurring methods with the proposed approach by using several objective assessment methods, including three kinds of reference image quality assessment (RIQA) techniques and one kind of blind image quality assessment (BIQA) approaches. In this paper, RIQA methods include the peak-signal-to-noise ratio (PSNR), structural similarity (SSIM) and multi-scale structural similarity (MSSSIM) (Wang *et al*., 2003). On the other hand, we also use the BIQA method for the analysis of the image quality (Liu *et al*., 2013). In all experiments, the following parameters are fixed: $\mu_0 = 4 \times e^{-2}$, $\lambda_0 = 4 \times e^{-3}$, $\beta_{\max} = 8$, $\alpha_{\max} = 1 \times e^3$ and $\gamma = 2$. The dark channel is computed in a neighborhood of 35×35.

5.1. Synthetic images. In this section, we quantitatively compare the performance of state-of-the-art deblurring methods with the proposed one on a data set with that of synthetically blurred images (Kohler *et al*., 2012). We use the set of 48 images generated from four images and 12 different kernels. The state-of-the-art deblurring methods (Cho and Lee, 2009; Xu and Jia, 2010; Kotera *et al*., 2017; Pan *et al*., 2018; Fergus *et al*., 2006) are used in the comparison.

Figure 3 shows the average PSNR, SSIM, and MSSSIM performance on this benchmark data set by some classical methods. According to these, the proposed method displays better performance than other techniques. It improves the method of Pan *et al*. (2018), and its performance is also robust. On the other hand, the analysis score of some examples by the BIQA method (Liu *et al*., 2013) is shown in Table 3. While the BIQA score of the image is small, the deblurring quality is low. From Table 3, the proposed algorithm yields a better score than other methods as for as the average score of all images is considered. Three images from this data set and their deblurred results are shown in Fig. 4. It is easy to see that the estimated kernel by most methods

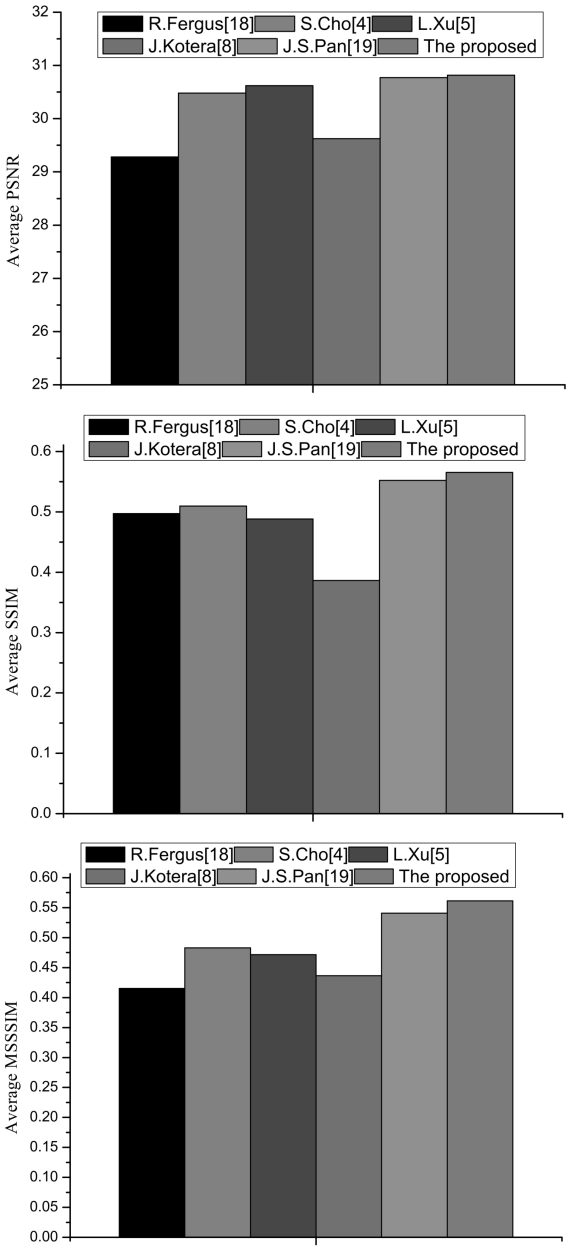

Fig. 3. Quantitative analysis of the data set of Kohler *et al.* (2012) based on the PSNR (top), SSIM (middle), and MSSSIM (bottom).

is close to the ground truth while the results by existing methods contain some noise (Cho and Lee, 2009; Fergus *et al*., 2006). The deblurred image by Kotera *et al*. (2017) has some ringing artifacts as shown in Fig. 4(f). Although deblurring methods (Xu and Jia, 2010; Pan *et al*., 2018) perform well for estimating the kernel, the performance of deblurring images is not good, and there are some artifacts in the images.

In addition, two images which contain many textures and the blur kernel with a large size are used as examples to further evaluate the performance of the proposed

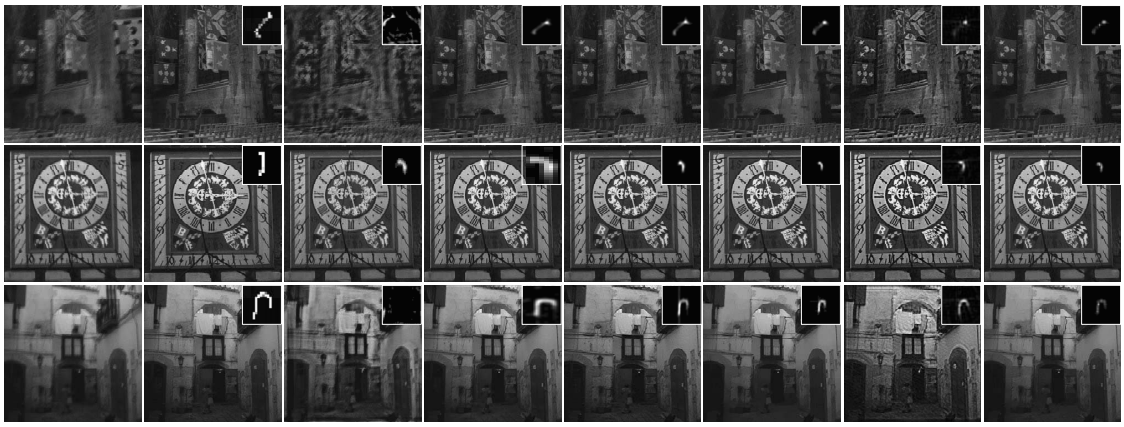

Fig. 4. Deblurring results on three images from the data set of Kohler *et al.* (2012). Note that the white frame in the top-right part of each image is the estimated kernel: blurry images (a), clear images and corresponding kernels (b), Fergus *et al.* (2006) (c), Cho and Lee (2009) (d), Xu and Jia (2010) (e), Kotera *et al.* (2017) (f), Pan *et al.* (2018) (g), proposed method (h).

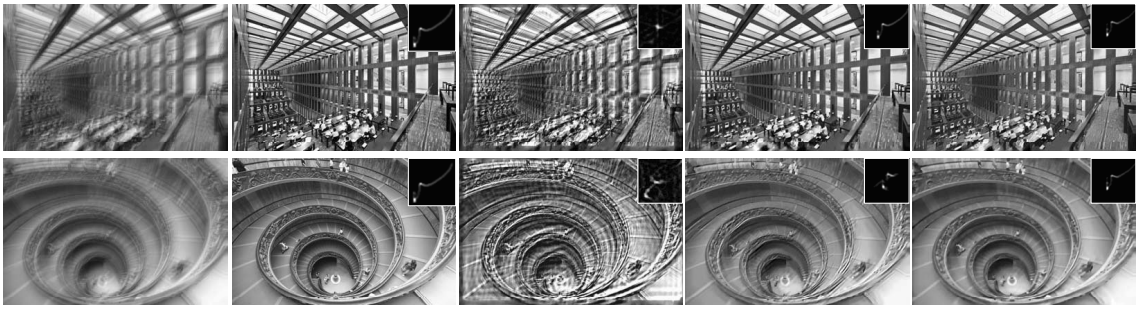

Fig. 5. Deblurring results on two images from the data set of Lai *et al.* (2016). Note that the white frame in the top-right part of each image is the estimated kernel: blurry images (a), clear images and corresponding kernels (b), Kotera *et al.* (2017) (c), Pan *et al.* (2018) (d), proposed method (e).

Table 1. Blind image quality assessment of several deblurring methods on the data set of Kohler *et al.* (2012).

Methods	Average BIQA
Fergus *et al.* (2006)	−13.86
Cho and Lee (2009)	−11.53
Xu and Jia (2010)	−11.46
Kotera *et al.* (2017)	−13.66
Pan *et al.* (2018)	−11.41
Our method	−11.37

Table 2. BIQA evaluation of image deblurring results for the image of Fig. 6.

Methods	BIQA
Blurry image	−19.21
Xu and Jia (2010)	−15.67
Kotera *et al.* (2017)	−13.08
Pan *et al.* (2018)	−11.24
Our method	−10.67

method. Figure 5 shows deblurring results obtained by the proposed method and state-of-the-art ones (Pan *et al*., 2018; Kotera *et al*., 2017). It is noteworthy that the kernels estimated by the proposed method are clear and close to the ground truth. As shown in Fig. 5, the estimated kernels obtained by Pan *et al*. (2018) are incomplete, so that the details of deblurred images are not right. Respectively, the bottom image of Fig. 5(b) has some ringing artifacts in the details of people. The deblurred result obtained by Kotera *et al*. (2017) has serious ringing artifacts, as shown in Fig. 5(c).

5.2. Real image. In this section, a challenging real captured blurry image, whose name is 'boat', is used to evaluate the performance of the proposed method. We compare our approach with the state-of-the-art blind single image deblurring methods (Xu and Jia, 2010; Kotera *et al*., 2017; Pan *et al*., 2018). We quantitatively analyze the deblurred results by using the metrics of BIAQ

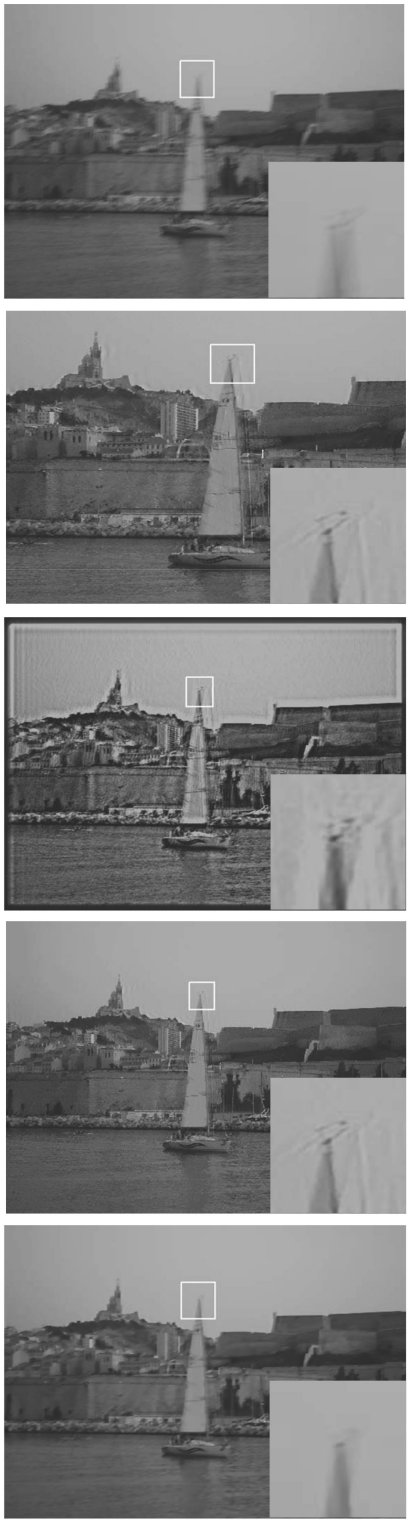

Fig. 6. Deblurring results of the boat image by the state-of-the-art deblurring methods (note that the bottom-right part of every result image is the high-resolution display of the white box in the image). From top to bottom: blurry image, Xu and Jia (2010), Kotera *et al.* (2017), Pan *et al.* (2018), proposed method.

because the blur kernels and the ground truth images of the blurry image are unknown. In addition, we also qualitatively analyze the deblurring results.

Figure 6 shows the deblurring results of the 'boat' image. The deblurring image with the proposed method applied is sharper and clearer than the results of other methods. Those contain ringing artifacts, as shown in the zoomed-in region of Fig. 6. The proposed method generates clearer edges and decreases the ringing artifacts. In addition, we present the BIAQ values of the images of Fig. 6 in Table 2.

5.3. Robustness in a blurry image with noise. As mentioned, the proposed method can be used to process synthetic and real images robustly. Because fractional order can inhibit the noise of the image and retain the texture of the image, the FODCP exhibits better performance in the blurry-noise image than the DCP. To demonstrate the effect of the image with noise on the proposed method, we quantitatively compare it with the approach by Pan *et al*. (2018) on the example image in Fig. 7. The variance of the Gaussian noise is varied from 0.01 to 0.06.

Figure 7 shows some deblurring results of the blurry image with different noise levels for the proposed method and that of Pan *et al*. (2018). Note that the proposed approach performs favorably against the state-of-the-art deblurring method since the dark channel prior is improved. As shown in Fig. 7, the deblurring results using the method of Pan *et al*. (2018) contain more and more noise when the noise level is increased. Although the PSNR of the deblurring results by the proposed method is decreasing with the noise level increasing, our approach exhibits favorable performance on the noise-blurry images.

5.4. Effectiveness of different parameters. Taking the data set of Kohler *et al*. (2012) and that of Levin *et al*. (2009) as examples, we explore the performance of the proposed method with different parameters after using various image quality measurement methods (PSNR and SSIM). Here, we mainly consider the parameters of the proposed method, including the image-gradient regularization term λ_0 and the FODCP regularization term μ_0, and the size of the local patch Ω in the FODCP. It is to be noted that $\beta_{\max}$ and $\alpha_{\max}$ should be set as very large according to Eqn. (23). Thus, $\beta_{\max}$ and $\alpha_{\max}$ are respectively set as 8 and $1 \times e^3$, which should be bigger than the value of μ_0 and λ_0.

5.4.1. Image-gradient regularization term λ_0. The parameter λ_0 is employed mainly to constrain the sparsity of the image gradient, which improves the quality of the restored images. Thus, we use the PSNR and SSIM to

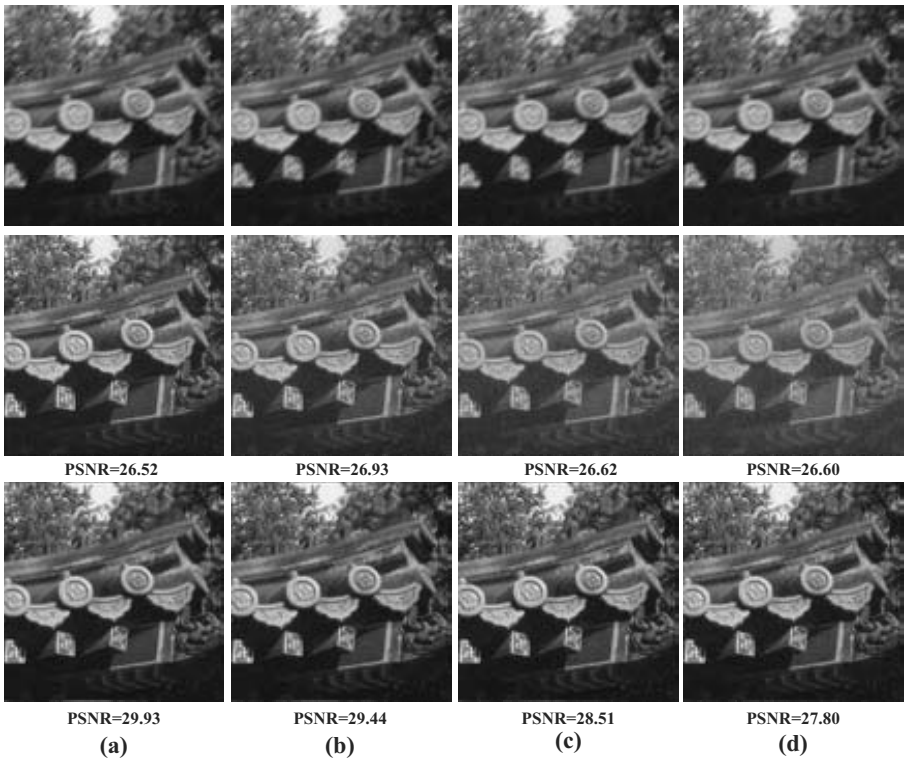

Fig. 7. Some deblurring results of blurry images which are corrupted with Gaussian noise with variance $\sigma = 0.01$ (a), variance $\sigma = 0.02$ (b), variance $\sigma = 0.04$ (c), variance $\sigma = 0.06$ (d). Note that the PSNR information denotes the quality of image. The first row denotes the blurry image with a different level noise. The second row denotes the deblurring results using the method of Pan *et al.* (2018) of the corresponding images in the first row. Similarly, the third row denotes the deblurring results using the proposed method.

evaluate the restored image. Here, λ_0 is set from $4e^{-4}$ to 10. However, the optimization of the proposed algorithm would be divergent when λ_0 is set as more than 1. As shown in Fig. 8(a), when $\lambda_0 = 4e^{-3}$, the proposed method can produce the best performance.

5.4.2. FODCP regularization term μ_0. The parameter μ_0 is employed mainly to constrain the sparsity of dark-channel result. Here, μ_0 is set from $4e^{-3}$ to 4. As shown in Fig. 8(b), when $\mu_0 = 4e^{-2}$, the proposed method can yield the best performance.

5.4.3. Size of the local patch Ω in the FODCP. To select the appropriate size of the local patch Ω in the FODCP, we evaluate the quality of the data set of Levin *et al*. (2009) based on the proposed method with different sizes of Ω. Here, the sizes of Ω is set from 15×15 to 55×55. The quantitative evaluation of the proposed method with different sizes of Ω is shown in Table3. It is clear that the proposed method can yield the best results (including the PSNR and SSIM) when the size of Ω is set as 35×35. Meanwhile, time consumption will be high when the size of Ω is set large. Therefore, we set the size of Ω as 35×35 in this paper.

5.5. Limitations. Although the proposed method can improve the deblurring performance of blurry images with noise, it will be ineffective when the noise level is too large. As shown in Fig. 9, our method outperforms that by Pan *et al*. (2018). When the blurry image is subjected to noise, the dark channel is destroyed, and the method of Pan *et al.* (2018) does not perform well. Although our approach exhibits favorable performance on the noisy blurry image, the PSNR of deblurring results by our method is decreasing when the noise level increases. It is clear that the proposed method exhibits poor performance for large image noise levels. Figure 10 shows a blurred image with very severe Gaussian noise. The proposed method generates the deblurring result still with significant noise. Therefore, our future work will consider a better denoising and deblurring method for this problem.

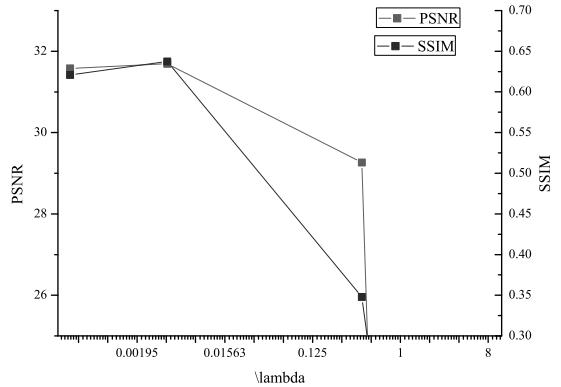

(a) parameter λ_0

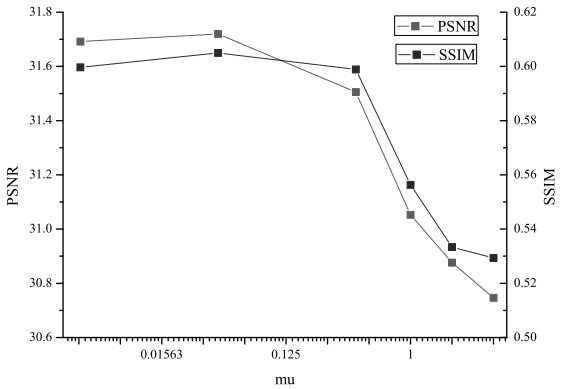

(b) parameter μ_0

Fig. 8. Effectiveness of the proposed method with different parameters on the data set of Kohler *et al.* (2012).

6. Conclusion

In this paper, we discussed the disadvantage of the dark channel prior and proposed a simple and effective improvement in the dark channel prior for image deblurring. Our fractional order dark channel prior can yield an effective dark channel of the blurry and intermediate images simultaneously since it can restrain the noise and enhance the texture. Furthermore, we also optimized the minimization problem of the sparsity of the fractional order dark channel prior by the half-quadratic splitting method. The experimental results, which are evaluated by some metrics, show that the proposed method is effective and robust for single deblurring in synthetic and real images.

Acknowledgment

This work was supported by the Key-Area Research and Development Program of Guangdong Province under the grant 2018B010108001, as well as the Science and Technology Plan Project of Jiangmen (2020030103080008999).

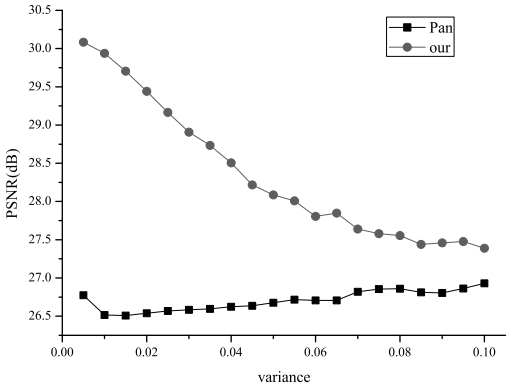

Fig. 9. Effectiveness of the proposed method on blurry images with different noise levels.

Table 3. Image quality assessment for the proposed method with different sizes of Ω on the data set of Levin *et al.* (2009).

Size of Ω	PSNR	SSIM	Time(s)
15×15	33.09	0.7552	107.80
25×25	33.28	0.7545	133.20
35×35	33.39	0.7656	171.44
45×45	33.23	0.7471	231.33
55×55	33.19	0.7519	274.08

References

An, S., Roh, H. and Kang, M. (2020). Long-term residual blending network for blur invariant single image blind deblurring, *arXiv:* 2007.04543.

Cho, S. and Lee, S. (2009). Fast motion deblurring, *ACM SIGGRAPH Asia* **28**(5): 1–8.

Fergus, R., Singh, B., Hertzmann, A., Roweis, S.T. and Freeman, W.T. (2006). Removing camera shake from a single photograph, *ACM Transactions on Graphics* **25**(3): 787–794.

Fuhai, C., Rongrong, J., Chengpeng, D., Xiaoshuai, S., Chia-Wen, L., Jiayi, J., Baochang, Z., Feiyue, H. and Liujuan, C. (2019). Semantic-aware image deblurring, *arXiv:* 1910.03853.

Gao, D., Liu, J., Wu, R., Cheng, D., Fan, X. and Tang, X. (2019). Utilizing relevant RGB-D data to help recognize RGB images in the target domain, *International Journal of Applied Mathematics and Computer Science* **29**(3): 611–621, DOI: 10.2478/amcs-2019-0045.

Gong, D., Yang, J., Liu, L., Zhang, Y., Reid, I., Shen, C., Van Den Hengel, A. and Shi, Q. (2017). From motion blur to motion flow: A deep learning solution for removing heterogeneous motion blur, *2017 IEEE Conference on Computer Vision and Pattern Recognition (CVPR), Honolulu, USA*, pp. 3806–3815.

He, K., Sun, J. and Tang, X. (2009). Single image haze removal using dark channel prior, *2009 IEEE Conference on Computer Vision and Pattern Recognition, Miami, USA*, pp. 1956–1963.

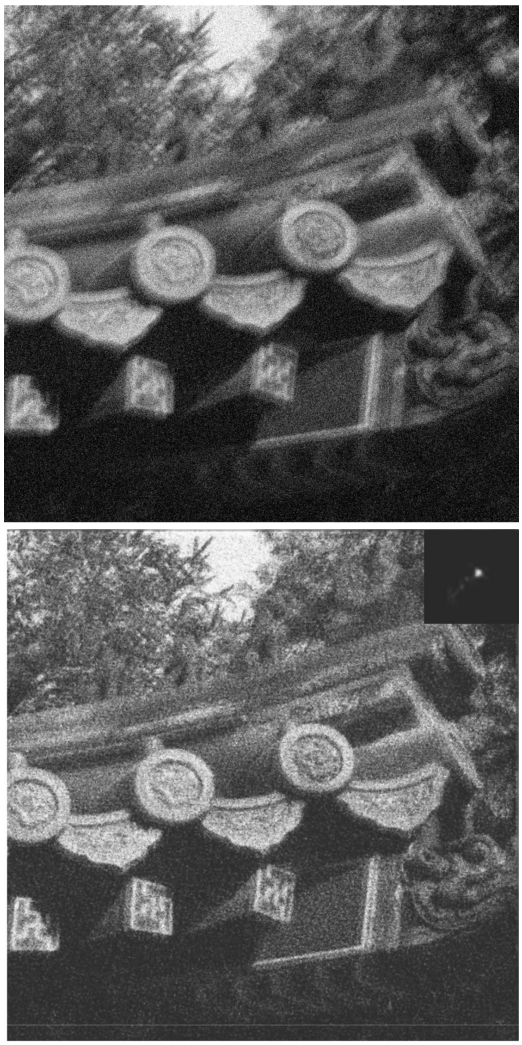

Fig. 10. Example of a blurry image with a large noise level: blurry image corrupted with Gaussian noise with variance $\sigma = 0.2$ (top), deblurring result by the proposed method (bottom).

Jia, H. and Pu, Y. (2008). Fractional calculus method for enhancing digital image of bank slip, *2008 Congress on Image and Signal Processing, Sanya, China*, Vol. 3, pp. 326–330.

Joshi, N., Zitnick, C.L., Szeliski, R. and Kriegman, D.J. (2009). Image deblurring and denoising using color priors, *2009 IEEE Conference on Computer Vision and Pattern Recognition, Miami, USA*, pp. 1550–1557.

Kohler, R., Hirsch, M., Mohler, B., Scholkopf, B. and Harmeling, S. (2012). Recording and playback of camera shake: Benchmarking blind deconvolution with a real-world database, *2012 European Conference on Computer Vision, Florence, Italy*, pp. 27–40.

Kotera, J., Smidl, V. and Sroubek, F. (2017). Blind deconvolution with model discrepancies, *IEEE Transactions on Image Processing* **26**(5): 2533–2544.

Kotera, J., Šroubek, F. and Milanfar, P. (2013). Blind deconvolution using alternating maximum a posteriori estimation with heavy-tailed priors, *in* R. Wilson *et al.* (Eds), *Computer Analysis of Images and Patterns*, Springer, Berlin/Heidelberg, pp. 59–66.

Kupyn, O., Budzan, V., Mykhailych, M., Mishkin, D. and Matas, J. (2018). DeblurGAN: Blind motion deblurring using conditional adversarial networks, *2018 IEEE/CVF Conference on Computer Vision and Pattern Recognition, Salt Lake City, USA*, pp. 8183–8192.

Lai, W.-S., Ding, J.-J., Lin, Y.-Y. and Chuang, Y.-Y. (2015). Blur kernel estimation using normalized color-line priors, *2015 IEEE Conference on Computer Vision and Pattern Recognition (CVPR), Boston, USA*, pp. 64–72.

Lai, W.S., Huang, J.B., Hu, Z., Ahuja, N. and Yang, M.H. (2016). A comparative study for single image blind deblurring, *2016 IEEE Conference on Computer Vision and Pattern Recognition (CVPR), Las Vegas, USA*, pp. 1701–1709.

Levin, A., Weiss, Y., Durand, F. and Freeman, W.T. (2009). Understanding and evaluating blind deconvolution algorithms, *2009 IEEE Conference on Computer Vision and Pattern Recognition, Miami, USA*, pp. 1964–1971.

Levin, A., Weiss, Y., Durand, F. and Freeman, W.T. (2011). Efficient marginal likelihood optimization in blind deconvolution, *2011 IEEE Conference on Computer Vision and Pattern Recognition, Colorado Springs, USA,* pp. 2657–2664.

Li, B. and Xie, W. (2015). Adaptive fractional differential approach and its application to medical image enhancement, *Computers & Electrical Engineering* **45**(C): 324–335.

Li, B. and Xie, W. (2016). Image denoising and enhancement based on adaptive fractional calculus of small probability strategy, *Neurocomputing* **175**(Part A): 704 – 714.

Li, J. and Lu, W. (2016). Blind image motion deblurring with ℓ_0-regularized priors, *Journal of Visual Communication & Image Representation* **40**(Part A): 14–23.

Li, P., Prieto, L., Mery, D. and Flynn, P.J. (2019). On low-resolution face recognition in the wild: Comparisons and new techniques, *IEEE Transactions on Information Forensics and Security* **14**(8): 2000–2012.

Liu, Y., Wang, J., Cho, S., Finkelstein, A. and Rusinkiewicz, S. (2013). A no-reference metric for evaluating the quality of motion deblurring, *ACM Transactions on Graphics* **32**(6): 175:1–175:12.

Matychyn, I. and Onyshchenko, V. (2021). Time-optimal control of linear fractional systems with variable coefficients, *International Journal of Applied Mathematics and Computer Science* **31**(3): 375–386, DOI: 10.34768/amcs-2021-0025.

Pan, J., Hu, Z., Su, Z. and Yang, M.H. (2014a). Deblurring text images via ℓ_0-regularized intensity and gradient prior, *2014 IEEE Conference on Computer Vision and Pattern Recognition, Columbus, USA*, pp. 2901–2908.

Pan, J., Liu, R., Su, Z. and Liu, G. (2014b). Motion blur kernel estimation via salient edges and low rank prior, *2014 IEEE International Conference on Multimedia and Expo (ICME), Chengdu, China*, pp. 1–6.

Pan, J., Sun, D., Pfister, H. and Yang, M. (2018). Deblurring images via dark channel prior, *IEEE Transactions on Pattern Analysis and Machine Intelligence* **40**(10): 2315–2328.

Ren, W., Cao, X., Pan, J., Guo, X., Zuo, W. and Yang, M.H. (2016). Image deblurring via enhanced low-rank prior, *IEEE Transactions on Image Processing* **25**(7): 3426–3437.

Shan, Q., Jia, J. and Agarwala, A. (2008). High-quality motion deblurring from a single image, *ACM Transactions on Graphics* **27**(3): 1–10.

Sun, L., Cho, S., Wang, J. and Hays, J. (2013). Edge-based blur kernel estimation using patch priors, *IEEE International Conference on Computational Photography (ICCP), Cambridge, USA*, pp. 1–8.

Wang, H., Pan, J., Su, Z. and Liang, S. (2018). Blind image deblurring using elastic-net based rank prior, *Computer Vision and Image Understanding* **168**: 157–171.

Wang, Z., Simoncelli, E.P. and Bovik, A.C. (2003). Multiscale structural similarity for image quality assessment, *37th Asilomar Conference on Signals, Systems Computers, Pacific Grove, USA*, Vol. 2, pp. 1398–1402.

Chen, X., Yang, Q.W. and Wu, J. (2010). Image deblur in gradient domain, *Optical Engineering* **49**(11): 49–49–7.

Xie, Z. (2016). A primal-dual method with linear mapping for a saddle point problem in image deblurring, *Journal of Visual Communication & Image Representation* **42**: 112–120.

Xu, L. and Jia, J. (2010). Two-phase kernel estimation for robust motion deblurring, *Proceedings of the 11th European Conference on Computer Vision: ECCV'10, Heraklion, Crete, Greece,* Part I, pp. 157–170.

Xu, L., Zheng, S. and Jia, J. (2013). Unnatural L_0 sparse representation for natural image deblurring, *2013 IEEE Conference on Computer Vision and Pattern Recognition, Portland, USA*, pp. 1107–1114.

Yan, Y., Ren, W., Guo, Y., Wang, R. and Cao, X. (2017). Image deblurring via extreme channels prior, *2017 IEEE Conference on Computer Vision and Pattern Recognition (CVPR), Honolulu, USA*, pp. 6978–6986.

Yin, M., Gao, J., Tien, D. and Cai, S. (2014). Blind image deblurring via coupled sparse representation, *Journal of Visual Communication & Image Representation* **25**(5): 814–821.

Zhang, H., Dai, Y., Li, H. and Koniusz, P. (2019). Deep stacked hierarchical multi-patch network for image deblurring, *Proceedings of the IEEE/CVF Conference on Computer Vision and Pattern Recognition (CVPR), Long Beach, USA,* pp. 5971–5979.

Zhichao, F., Yingbin, Z., Hao, Y., Yu, K., Jing, Y. and Liang, H. (2019). Edge-aware deep image deblurring, *arXiv:* 1907.02282.

Zhong, L., Cho, S., Metaxas, D., Paris, S. and Wang, J. (2013). Handling noise in single image deblurring using directional filters, *2013 IEEE Conference on Computer Vision and Pattern Recognition, Portland, USA*, pp. 612–619.

Xiaoyuan Yu was born in 1991. He received his PhD degree in the Department of Physics and Optoelectronic Engineering of the Guangdong University of Technology, China, in 2013, his MS degree in the Department of Physics and Telecommunications Engineering of South China Normal University, Guangzhou, China, in 2016, and his PhD degree in the College of Automation Science and Engineering of the South China University of Technology in 2021. Now, he is working as a postdoctoral researcher at the Soft College of the South China University of Technology. His current research interests include image processing and computer vision.

Wei Xie was born in 1974. He received his BS and MS degrees in the Automation Department of the Wuhan University of Science and Technology, China, in 1996 and 1999, respectively, and his PhD degree from the Kitami Institute of Technology, Japan, in 2003. He worked as a postdoctoral researcher at the Satellite Venture Business Laboratory from 2003 to 2006. In 2006, he joined the College of Automation Science and Engineering, South China University of Technology, as an associate professor and was promoted to be a full professor in 2010. He is an inventor/co-inventor of numerous Chinese patents. His research interests are in robust control theory and application, gain scheduling control, pattern recognition, computer control and application, and video information processing.

Jinwei Yu was born in 1995. He received his BEng degree in the College of Automation Science and Engineering from the South China University of Technology, Guangzhou, China, in 2019. He is currently a PhD candidate there. His present research interests include image processing and computer vision.

Received: 3 October 2021
Revised: 29 January 2022
Re-revised: 5 March 2022
Accepted: 5 March 2022